Influence of Corrosion Pits on the Fatigue Limit of 12% Cr Steam Turbine Blade Steel

B. Schönbauer [1,a], S. Stanzl-Tschegg [1,b], N. Rieger [2,c], R. Salzman [2,d] and D. Gandy [3,e]

[1] University of Natural Resources and Life Sciences (BOKU),

Peter-Jordan Straße 82, A-1190 Vienna, Austria

[2] STI Technologies Inc., Simutech Group,

1800 Brighton-Henrietta Townline Rd., Rochester, NY, 14623 USA

[3] Electric Power Research Institute (EPRI),

1300 West W.T. Harris Boulevard, Charlotte, NC 28262 USA

[a] bernd.schoenbauer@boku.ac.at, [b] stefanie.tschegg@boku.ac.at,

[c] nrieger@SimuTechGroup.com, [d] rsalzman@SimuTechGroup.com, [e] davgandy@epri.com

Keywords: Pitting Corrosion; Very High Cycle Fatigue; Fatigue Crack Growth; 12%Cr Martensitic Steel

Abstract. Fatigue failure of steam turbines emanating from corrosion pits is still an issue for power plant operators today, even after decades of research to understand the phenomenon. In this work, the results of fatigue tests in the very high cycle fatigue regime are presented to quantitatively describe the influence of corrosion pits on the fatigue limit. The test material was dual certified 403/410 12% Cr martensitic steel which is commonly used for steam turbine blades in the low pressure region of the steam turbine where pitting corrosion preferentially occurs.
Fatigue crack growth rate (FCGR) measurements for both long cracks in the near threshold regime and cracks that were initiated at corrosion pits were performed. Additionally, S-N tests with smooth and pre-pitted specimens were carried out. The results were correlated in Kitagawa-Takahashi diagrams with the use of the approach of El Haddad and co-workers for short cracks. Furthermore, the influence of the stress ratio was investigated for both threshold stress intensity factor range ΔK_{th} and fatigue limit $\Delta\sigma_{th}$. With these results, the fatigue limit of specimens showing corrosion pits can be evaluated for any value of stress ratio ($R \geq -1$).

Introduction

Corrosion pits as crack initiation sites are a well know problem for operators of steam turbines. Failure of low pressure steam turbine blades due to corrosion fatigue has often been observed during the last decades and therefore numerous investigations have been conducted (e.g. [1,2]). In case of undefined conditions, such as shut down of the turbine and leaking of the condenser, the presence of oxygen and chloride accelerates pitting corrosion. If a pit exceeds a critical size, the increase of the local stresses can initiate a fatigue crack which, under adverse conditions, can lead to final failure.

In this work, 12% Cr martensitic steel, which is a standard material for steam turbine blades in the low pressure part, was used as testing material to observe the influence of corrosion pits on the fatigue behaviour. S-N tests as well as fatigue crack growth rate (FCGR) measurements in the near

threshold regime were performed using ultrasonic fatigue testing equipment with superimposed static load provided by a servo-hydraulic testing machine. The pit-to-crack transition was investigated with artificially generated corrosion pits and the results were correlated in Kitagawa-Takahashi diagrams.

During turbine blade operation, the dynamic stresses can be very low in relation to the mean stresses. Therefore, an extrapolation to stress ratios exceeding R=0.9 is necessary. While the fatigue limits for very high R-ratios can be estimated using established approximations, the threshold stress intensity values cannot be determined with sufficient accuracy. Therefore, additional fatigue crack growth rate measurements for different R-ratios between R=-1 and 0.9 were performed. With these results, Kitagawa-Takahashi diagrams for any stress ratio can be created. In addition, the fracture surfaces were observed and analysed to characterize the crack initiation mechanisms and to determine the geometry of the corrosion pits.

Material, Specimens and Testing Method

The testing material was dual certified 403/410 12% Cr martensitic steel which was heat treated in the following way: 913°C (1 h/water quenched) + 649°C (4 h/air cooled) + 621°C (4 h/air cooled). The chemical composition and the mechanical properties (provided by the supplier) are listed in Table 1 and 2. The mean grain size of the material was 6 µm.

Table 1. Chemical composition of 403/410 SS (in weight%)

C	Cr	Mn	Si	Ni	Mo	Cu	S	P
0,13-0,14	11,79-11,88	0,41-0,49	0,18-0,26	0,28-0,33	0,13-0,18	0,07-0,10	0,001-0,002	0,013-0,020

Table 2. Mechanical properties of 403/410 SS at room temperature

Tensile Strength [MPa]	Yield Strength [MPa]	Elongation [%]	Reduction of Area [%]
767	596	23	68

Specimens for S-N tests with a cylindrical gauge length of 10 mm (shown in Fig. 1a) were machined, ground and polished with abrasive paper (up to grade #4000) to obtain a mirror finish. To eliminate residual stresses, the specimens were stress-relief annealed in high vacuum at10^{-3} Pa (heating from room temperature to 600°C in one hour, holding for two hours, cooling from 600°C to 400°C in two hours and to room temperature in approx. 12 hours). Partly, artificial corrosion pits were introduced into the gauge length of the test specimens. The pre-pitting procedure was developed and arranged at the National Physical Laboratory in the UK [3] which allows producing single corrosion pits with a reproducible depth (± 10% of the targeted value). Pit depths of 50, 100 and 250 µm were used.

For FCGR measurements and determination of threshold stress intensity factors, tubular specimens with a starter notch were used (see Fig. 1b). Surface finish and stress-relief was identical with that of the dumbbell shaped specimens.

Fatigue measurements were performed using ultrasonic fatigue testing equipment with superimposed static load by the use of servo-hydraulic testing equipment for testing at higher stress ratios. The ultrasonic technique works by stimulating specimens to resonance vibrations at about 20 kHz cycling frequency, which allows to obtain more than 10^9 cycles within one day. Since the vibration amplitude is zero at the places of strain and stress maximum of the specimen, the failure location is stationary and can be observed during fatigue testing. Thus, crack initiation and propagation can be observed optically. For this purpose, an optical system with 250x magnification was used which allowed to detect crack elongations of less than 10 µm.

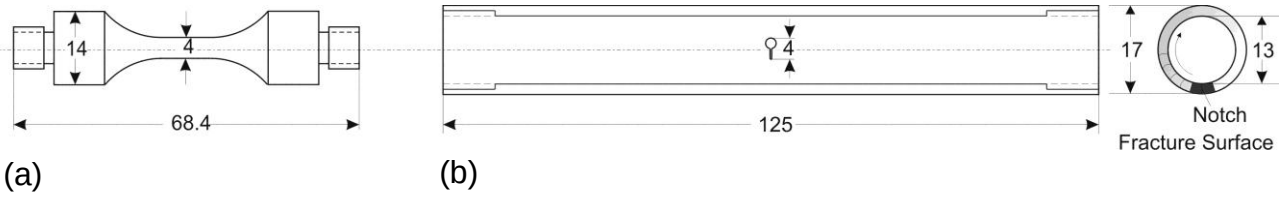

Fig.1. Shape of (a) fatigue specimens for S-N tests and (b) tubular specimens for fatigue crack growth measurements.

Experimental Results

The threshold stress intensity factor range ΔK_{th} was defined as the minimum value for which the observed crack does not advance after at least $1 \cdot 10^8$ cycles. The FCGR curves (Fig. 2a) showed the expected shift to higher crack growth rates and lower threshold ΔK_{th} with increasing stress ratio R. Near threshold FCGR test were performed for ten stress ratios (R=-1, 0.05, 0.3, 0.4, 0.5, 0.6, 0.7, 0.8, 0.85 and 0.9) and the results are shown in a ΔK_{th}-K_{max} diagram. For threshold values of the maximum stress intensity factor K_{max} above 10 MPa√m no further decrease of ΔK_{th} was visible.

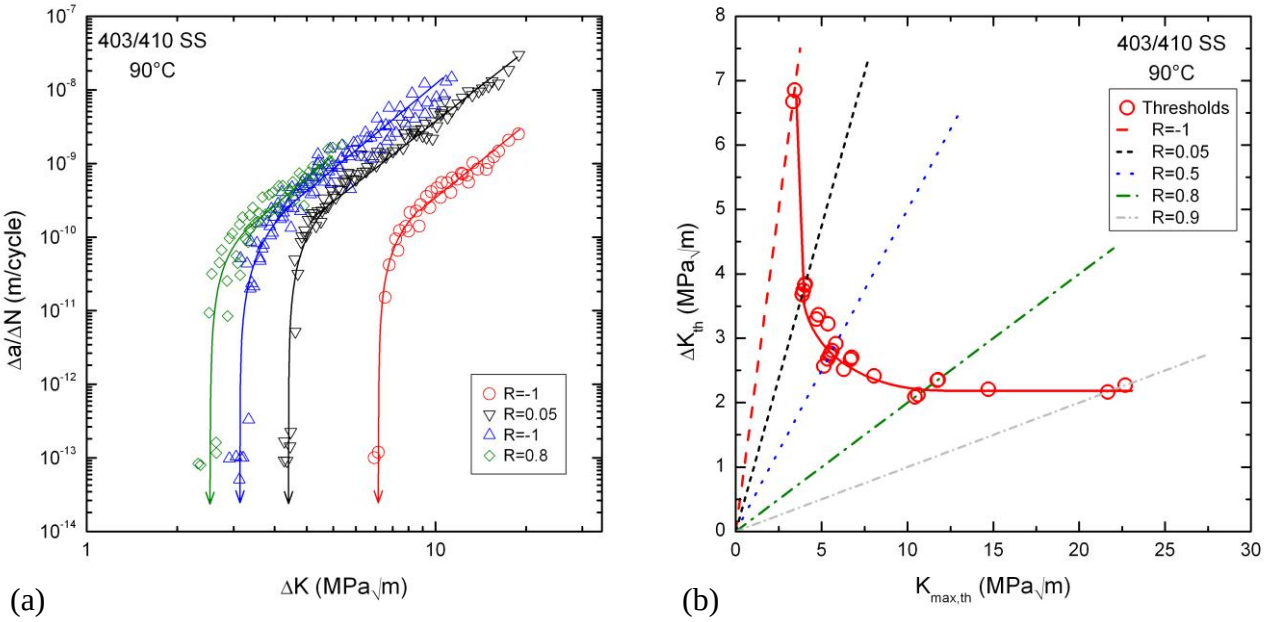

Fig.2. (a) FCGR curves at stress ratios of -1, 0.05, 0.5 and 0.8 and (b) ΔK_{th}-K_{max} for multiple stress ratios

S-N tests were performed on specimens with and without pre-pitting. In the present work, the fatigue limit $\Delta\sigma_0$ was defined as the cyclic stress range which does not cause failure within at least $1 \cdot 10^9$ cycles. At a stress ratio of 0.05 and 0.5 and 0.8, fatigue tests were conducted on smooth specimens. In addition, fatigue tests on pre-pitted specimens with pit depths of 50, 100 and 250 µm deep pits were performed. The S-N curves for both, smooth and pre-pitted specimens are shown in Figure 3a.

For smooth specimens, mainly non-metallic inclusions were found at crack initiation sites. An example is shown in Figure 3b where the fatigue crack started at an Al_2O_3 inclusion at the surface. With higher values of stress ratio, an increase of the critical pit size (minimum pit size leading to initiation of propagating cracks) was observed. For R=0.05, the nucleation of fatigue cracks which led to failure was located at the corrosion pit exclusively (minimum pit depth of 50 µm). For a stress ratio of 0.5 and a pit depth of 50 µm, the crack initiation site of one failed specimen was the pit while it was elsewhere for another one. Although non-propagating short cracks were found at pits with depths 100 µm for R=0.8, none of these cracks caused final failure. The reason for this is most probably enhanced local plastic deformation around the pits at higher stress ratios.

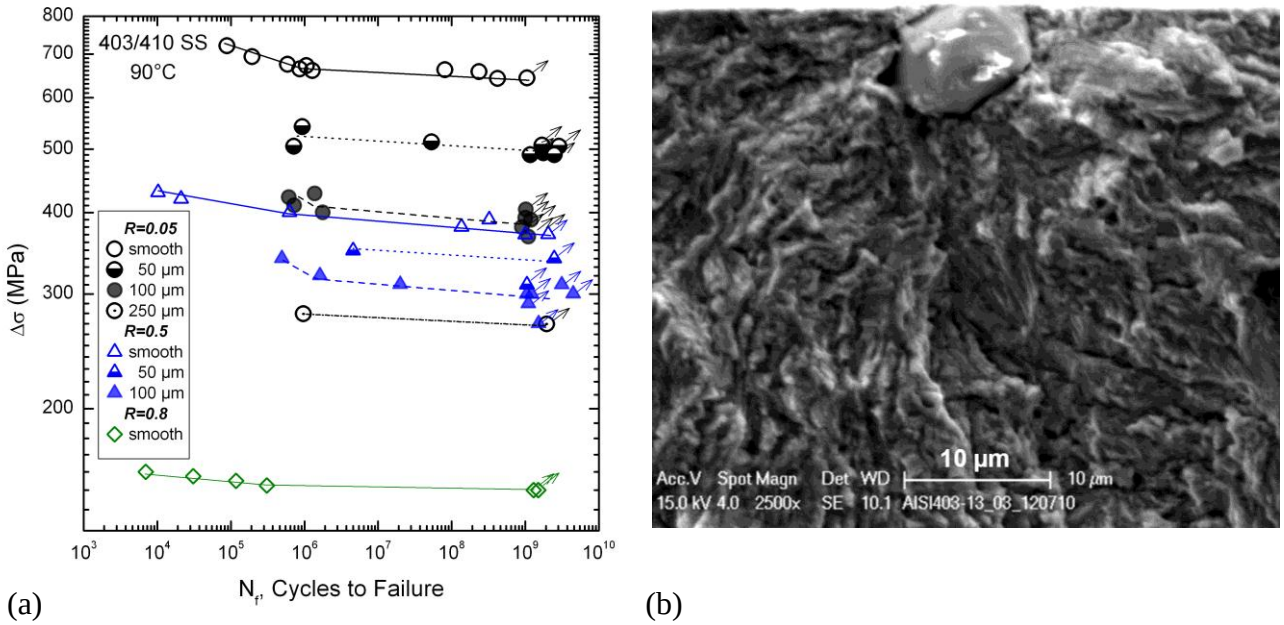

(a) (b)

Fig.3. (a) S-N curves for smooth and pre-pitted specimens. (b) Fracture surface with Al_2O_3 inclusion as crack initiation site (R=0.05, $\Delta\sigma$=642 MPa, $N_f=1.06 \cdot 10^6$ cycles).

Furthermore, crack initiation at corrosion pits was observed and FCGR measurements were performed. The stress intensity factor was calculated by assuming a semi-circular crack shape with a radius of a, which is half of the surface crack length including the pit diameter (Fig. 4b). The incipient cracks at the corrosion pits showed the typical behaviour of short cracks: At stress intensity factor ranges below the threshold, initial crack propagation was observed. With increasing crack length, the crack growth rates coincide with the curve for long cracks. Below the fatigue limit of pre-pitted specimens, fatigue cracks can form but become non-propagating. In Figure 4a, FCGR curves for both long cracks and cracks initiated at corrosion pits are shown.

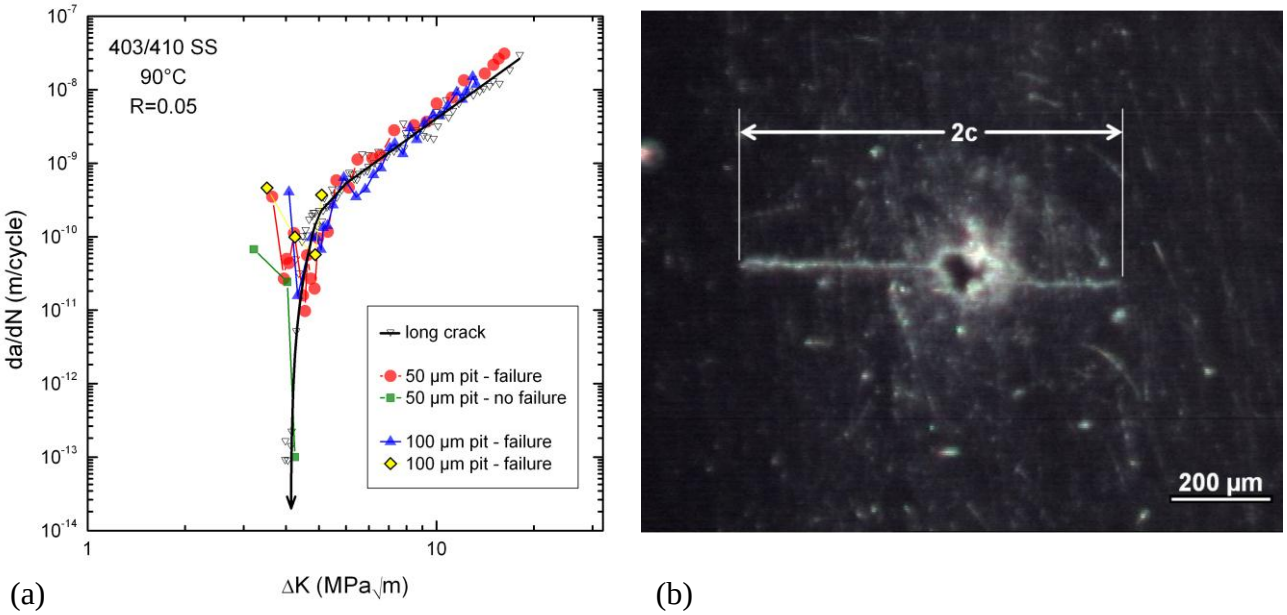

(a) (b)

Fig.4. (a) FCGR curves for cracks that initiated at corrosion pits (R=0.05). (b) Fatigue crack at an 100µm deep corrosion pit (R=0.05, Δσ=428 MPa)

The values of the threshold stress intensity factor ranges, ΔK_{th}, and the fatigue limit for smooth and pre-pitted specimens, $\Delta\sigma_0$ and $\Delta\sigma_{0,\text{pit size}}$, are summarized in Table 3.

Table 3. Threshold stress intensity factor ranges and fatigue limits at 90°C.

R	ΔK_{th} [MPa√m]	$\Delta\sigma_0$ [MPa]	$\Delta\sigma_{0,50\mu m}$ [MPa]	$\Delta\sigma_{0,100\mu m}$ [MPa]	$\Delta\sigma_{0,250\mu m}$ [MPa]
-1	6.77	-	-	-	-
0.05	3.76	630	490	390	270
0.5	2.74	370	340	300	-
0.8	2.23	150	-	-	-

Discussion

To evaluate the influence of corrosion pits on the fatigue limit, linear elastic fracture mechanics (LEFM) is used. Therefore, the pits are treated as effective cracks, which is a well-established method (e.g. [4,5]). Observation of the fracture surface showed that most pits have roughly a semi-elliptical shape with an approximately equal value for the pit width at the surface, 2c, and the pit depth, a (see Fig. 5a). Nevertheless, it was found that the pits can be treated as semi-circular surface cracks with a radius of half of the pit width at the surface, which was discussed in more detail elsewhere [6]. With this approximation and the consideration that the pit size is small in terms of short crack behaviour, the stress intensity factor of corrosion pits can be calculated with following equation:

$$\Delta K = \Delta\sigma\sqrt{\pi\cdot(c+c_0)}\cdot Y\,. \qquad (1)$$

The geometry factor, Y, for semi-circular surface cracks is assumed to be 0.65 and c_0 depends on the material according to the empirical relationship proposed by El Haddad et al. [7]:

$$c_0 = \frac{1}{\pi} \cdot \left(\frac{\Delta K_{th,lc}}{Y \cdot \Delta\sigma_0} \right)^2 , \tag{2}$$

where $\Delta K_{th,lc}$ is the threshold stress intensity factor range for long cracks.

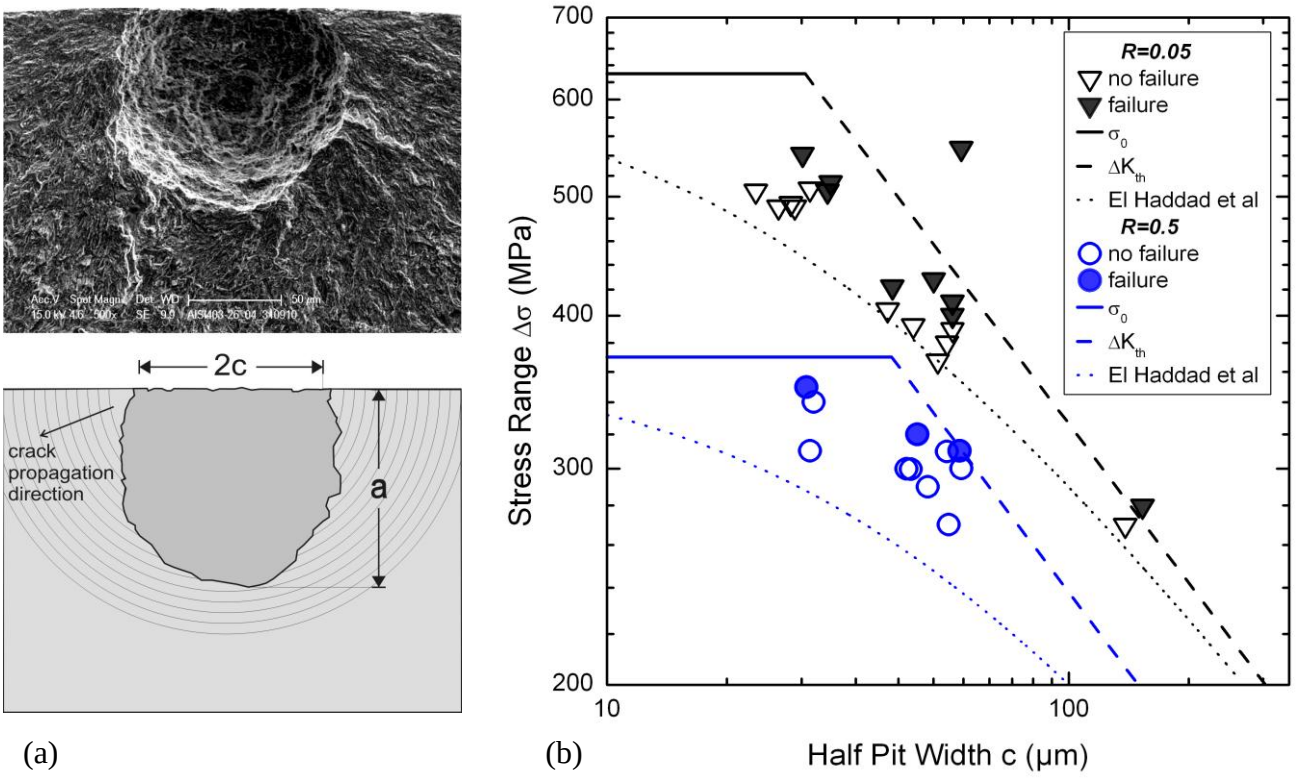

Fig.5. (a) Fracture surface with corrosion pit and schematic illustration of pit geometry.
(b) Kitagawa-Takahashi diagram showing the effect of pits on the fatigue limit.

The applicability of this approximation can be seen in Figure 5b, where the fatigue data of pre-pitted specimens are represented in a Kitagawa-Takahashi diagram. Failure was found below threshold stress intensity factor values for long cracks (dashed lines). Equations 1 and 2 (dotted lines) give a sufficient estimation for the fatigue limit of pitted specimens.

During operation of steam turbines, a wide range of stress ratios can occur and R-ratios can exceed 0.9. Therefore, it is necessary to extrapolate both ΔK_{th} and $\Delta\sigma_0$. In Figure 6a, the influence of stress ratio, R, on the threshold stress intensity factor range, $\Delta K_{th,}$ is plotted. Above a stress ratio of R=0.72, no further decrease of ΔK_{th} is found, which can be seen in Figure 2b, too. This is consistent with the model by Schmidt et al. [8] which is based on the concept of crack closure. The decrease of ΔK_{th} with R can be parameterized by following formulas:

$$\Delta K_{th} = 4.06 - 2.57 \cdot R, \qquad \text{if } R \leq 0.72 \tag{3}$$

$$\Delta K_{th} = \text{const.} = 2.22 \text{ MPa}\sqrt{\text{m}}, \qquad \text{if } R > 0.72. \tag{4}$$

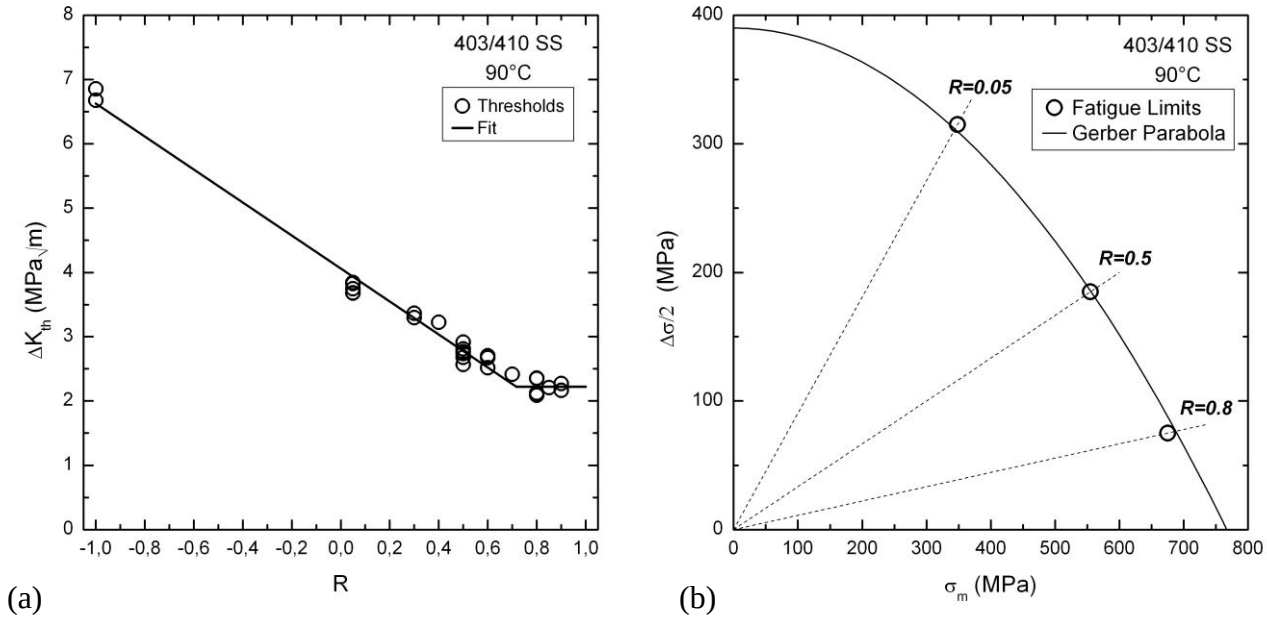

Fig.6. (a) Influence of stress ratio, R, on the FCGR threshold, ΔK_{th}. (b) Haigh diagram with parabolic fit.

To see the relationship between stress ratio, R, and fatigue limit, $\Delta\sigma_0$, data can be plotted in a Haigh diagram, see Figure 6b. For this purpose, the stress amplitude, $\Delta\sigma/2$, is plotted against the mean stress, σ_m. Assuming the fatigue limit for smooth specimens at R=-1, $\Delta\sigma_{0,R=-1}$, with 780 MPa, these results can be fitted with a Gerber Parabola (σ_u is the tensile strength):

$$\Delta\sigma_0 = \Delta\sigma_{0,R=-1} \cdot (1 - \sigma_m/\sigma_u)^2). \quad (5)$$

With equations 3-5, Kitagawa-Takahashi diagrams for all stress ratios, R, can be created and with addition of equations 1-2, the fatigue limit for pitted specimens are assessable.

Summary

Investigations with dual certified 403/410 12% Cr martensitic steel were performed to quantify the influence of corrosion pits on the fatigue life of this standard material for turbine blades in the low pressure part. FCGR measurements in the near threshold regime for multiple stress ratios (R=-1–0.9) were carried out. To define the fatigue limit of smooth and pre-pitted specimens, S-N tests in the VHCF regime were performed for three different values of R (0.05, 0.5 and 0.8). Additionally, FCGR curves were determined for short cracks that initiated at corrosion pits.

Following results were obtained:

- Kitagawa-Takahashi diagrams can be used for assessment of the fatigue limit, $\Delta\sigma_0$, for specimens showing pitting corrosion. For small pits, propagating cracks can be formed below threshold stress intensity factors for long cracks, $\Delta K_{th,lc}$. Therefore, the approach by El Haddad and co-workers for short surface cracks is appropriate.
- The relationship between threshold stress intensity factor range, ΔK_{th}, and stress ratio, can be fitted with two linear lines: a constant slope for $R \leq 0.72$ of ΔK_{th} with increasing R and a constant value of ΔK_{th}=2.2 MPa√m above R=0.72 was found.

- The dependency of the fatigue limit, $\Delta\sigma_{0,}$ on the stress ratio can be assessed by the use of a Gerber parabola.

With these results, Kitagawa-Takahashi diagrams for any value of R can be created and hence, the fatigue limit for pitted specimens can be obtained according to the operational condition of steam turbine blades.

Acknowledgement

The presented results were achieved during the first part of a program to develop a methodology for the prediction of corrosion fatigue life in steam turbine blades, being conducted by the Electric Power Research Institute (EPRI) of Charlotte NC.

References

[1] Jaffe, R.I.: Proceedings: *Corrosion Fatigue of Steam Turbine Blade Materials*, Electric Power Research Institute (EPRI), Palo Alto, California, 21-24 September 1981, Pergamon Press (1984).

[2] Speidel M.O., Atrens A.: *Corrosion in Power Generating Equipment*, Plenum Press NY, (1984).

[3] Salzman, R.N.: *Corrosion-Fatigue Prediction Methodology*, EPRI, Palo Alto, CA (2009), EP-P31022/C14387.

[4] Chen, G.S., Wand, K.-C., Gao, M., Wei, R.P., Flournoy, T.H.: Transition from Pitting to Fatigue Crack Growth – Modelling of Corrosion Fatigue Crack Nucleation in a 2024-T3 Aluminium Alloy, Material Science and Engineering A219 (1996), pp. 126-132.

[5] Zhou, S., Turnbull, A.: Influence of Pitting on the Fatigue Life of a Turbine Blade Steel, Fatigue Fract Engng Mater Struct 22 (1999), pp. 1083-1093.

[6] Schönbauer B., Stanzl-Tschegg, S., Rieger, N., Salzman, R., Turnbull, A., Zhou, S., Gandy, D.: Crack Initiation and Propagation in 12% Cr Steam Turbine Balde Steel, in: Proceedings of VHCF5, Berlin (2011), pp. 545-550.

[7] El Haddad, M.H., Topper, T.H., Smith, K.N.: *Fatigue Life Predictions of Smooth and Notched Specimens*, ASME Jnl Engrg Matls Technol 103 (1981), pp. 91-96.

[8] Schmidt, R.A., Paris, P.C.: *Threshold for Fatigue Crack Propagation and the Effect of Load Ratio and Frequency*, ASTM STP 536, ASTM, Philadelphia (1973), pp. 79-94.